Journal of Materials Chemistry A

Accepted Manuscript

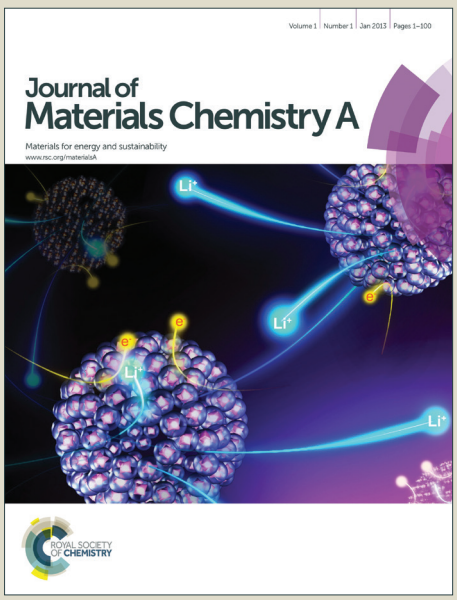

ROYAL SOCIETY OF CHEMISTRY

www.rsc.org/materialsA

Journal of Materials Chemistry A

ARTICLE

Received 00th January 20xx,

Accepted 00th January 20xx

DOI: 10.1039/x0xx00000x

www.rsc.org/

Ethanol-tolerant polyethyleneimine functionalized palladium nanowires in alkaline media: The "molecular window gauze" induced the selectivity for the oxygen reduction reaction†

Guang-Rui Xu,[a] Feng-Yi Liu,[b] Zong-Huai Liu [a] and Yu Chen[a]*

Owing to alcohol crossover problem, improving the selectivity of cathodic electrocatalysts for the oxygen reduction reaction (ORR) is one of the key challenges for the commercial viability of direct alcohol fuel cells. Pd is highly efficient Pt-alternative elelctrocatalyst for the ORR in alkaline media but it is also highly active for the alcohol oxidation reaction (AOR) in alkaline media. In this work, we demonstrate an efficient water-based synthesis of Pd nanowires (Pd-NWs) in presence of polyethyleneimine (PEI) with branched structure. Experimental results show the formation of Pd-NWs originates from oriented attachment. During the synthesis, Pd-NWs are simultaneously functionalized by PEI due to strong Pd-N interaction, which is confirmed by molecular dynamics simulation and various physical characterizations. PEI layers on Pd-NWs efficiently serve as "molecular window gauze" to physically block the access of alcohol molecules to Pd sites but allow the access of oxygen molecules owing to their difference in molecular size, resulting in excellent alcohol tolerance of Pd-NWs for the ORR in alkaline media. Our results provide a new strategy for the designing ethanol-tolerant noble metal electrocatalysts.

Introduction

Direct alcohol fuel cells (DAFCs) are electrochemical devices that act to directly transfer chemical energies of various alcohol molecules into electrical energy, which offer a sustainable and environmentally friendly alternative energy source to the combustion of fossil fuels for automotive and portable electronic devices.[1-3] Pt-based metal nanoparticles are the most widely used cathodic electrocatalysts for the oxygen reduction reaction (ORR).[4-7] However, the commercialization of DAFCs suffers from the alcohol crossover problem that causes the CO poison of cathodic Pt electrocatalysts and reduces fuel efficiency due to the alcohol oxidation on cathodic Pt.[8, 9] Recently, the stable and less expensive Pd has been widely exploited as the efficient Pt-alternative elelctrocatalysts for the ORR in alkaline media.[10-24] Unfortunately, similar to Pt in acidic media, Pd also has excellent intrinsic electrocatalytic activity for the alcohol oxidation reaction (AOR) in alkaline media.[16, 25-27] Thus, improving the selectivity of cathodic Pd electrocatalysts for the ORR in alkaline media is still anticipated.

Since the AOR involves the diffusion of alcohol molecules from solution to the active sites of electrocatalysts and adsorption-dissociation process of alcohol molecules on the surface of electrocatalysts, blocking diffusion and inhibiting adsorption are two mainly strategies for achieving the ORR selectivity. According to the mechanism of the AOR, three adjacent Pt sites are required for the AOR whereas two or less are needed for the ORR.[28-30] A recent excellent work demonstrated that the isolated Pt atom modified covalent triazine frameworks exhibited the good selective activity for the ORR even in the presence of high concentration of methanol.[30] However, the synthesis of the isolated Pt atom modified nanomaterials is very difficult. By means of the second element dilution effect, alloying Pt with second element may be a facile strategy for achieving the selectivity of Pt electrocatalysts for the ORR, which prevents alcohol molecules from adsorbing on the Pt sites while oxygen is not perturbed. For example, PtCo[28] and PdFe@PtPd core-shell[29] nanoparticles displayed high methanol tolerance in acidic media. Similarly, PdAg alloy nanorings exhibited the superior methanol tolerance for the ORR in alkaline media.[15]

Covering noble metal nanoparticles with the porous materials is another efficient route for improving ORR selectivity, which can physically block access of alcohol molecules to active sites due to the difference in molecular size between alcohol and oxygen. For example, the cage-bell structured Pt-Ru nanoparticles[31] and Pt@ordered mesoporous carbon frameworks composites[32] exhibited the good methanol tolerance for the ORR. In addition, by means of the difference in the alcohol solubility in different solvents, modifying electrocatalysts with liquid material with high oxygen solubility is also expected to achieve the ORR selectivity. For example, the graphene-Pt composites impregnated with the ionic liquid [MTBD][bmsi] showed excellent methanol tolerance for the ORR by preventing diffusion of methanol from water to [MTBD][bmsi] layers on Pt surface.[8]

[a] Key Laboratory of Macromolecular Science of Shaanxi Province, School of Materials Science and Engineering, Shaanxi Normal University, Xi'an 710062, PR China
E-mail: ndchenyu@gmail.com (Y. Chen)
[b] School of Chemistry & Chemical Engineering, Shaanxi Normal University, Xi'an 710062, P.R. China

† Electronic Supplementary Information (ESI) available: Experimental details and additional physical characterization. See DOI: 10.1039/x0xx00000x

More recently, by virtues of chemical interaction between the noble metal nanoparticles and the functional molecules, the surface chemical functionalization of noble metal nanoparticles with specific molecules has also emerged as a promising strategy for tuning the electrocatalytic activity and selectively. For example, calix [4] arene functionalized Pt could selectively electrocatalyze the hydrogen oxidation reaction in the presence of oxygen molecule.[33, 34] Our recent work also demonstrated the polyallylamine functionalized Pd icosahedra [35] had excellent selectivity for the ORR in the presence of alcohol. However, the polyallylamine functionalized Pd icosahedra suffered from the tedious UV/ozone post-treatment procedure, prior to the electrocatalytic application.

Apart from the activity and selectivity, improving the durability of cathodic electrocatalyts for the ORR is a key issue for maintaining the performance of DAFCs. Recent advances[36-43] reveal that one-dimensional (1D) Pd nanowires (Pd-NWs) generally show enhanced electrocatalytic activity for small molecule oxidation or reduction due to their unique structure properties, including large surface-to-volume ratio, excellent electron transport, and good mass transport of reactant, *etc*. Meanwhile, Pd-NWs have superior electrochemical stability because no individual Pd nanoparticle exists in such 1D nanostructures, which efficiently restrains the Ostwald ripening effect and consequently retains their electrochemical active surface area (ECSA).

In this work, we demonstrate a very facile and efficient chemical reduction route to synthesize the polyethyleneimine (PEI, Scheme S1 in ESI†) functionalized Pd nanowires (Pd-NWs@PEI) with a high yield in aqueous solution, which can be directly used as cathodic electrocatalyst without tedious post-treatment prodcure. The loosely packed PEI layers on Pd-NWs surface effectively act as "molecular window gauze" to physically block access of alcohol molecules to Pd sites, resulting in the good ORR selectivity of Pd-NWs@PEI in the presence of ethanol in alkaline media. Meanwhile, the as-prepared Pd-NWs@PEI also show the improved electrocatalytic activity and stability for the ORR compared to commercial Pd black.

Experimental section

Preparation of Pd-NWs@PEI

In a typical synthesis, 0.9 mL of 0.05 M polyethyleneimine (PEI, Scheme S1 in ESI†, M_w≈10000) and 1.0 mL of 0.05 M K_2PdCl_4 aqueous solutions were added into 8.1 mL water. After adjusting the solution pH to 11.0, the mixture solution was heated to 80 ^oC under vigorous magnetic stirring. Then, 0.5 mL of $N_2H_4{\cdot}H_2O$ (85%) was rapidly added to the mixture and further mechanically stirred for 2 h. Finally, the products were collected by centrifugation at a rate of 10000 rpm for 10 min, completely washed with water, and dried at 50 ^oC in a vacuum.

Electrochemical measurements

Electrochemical tests were carried on a CHI 660 D electrochemical workstation with a Gamry RDE710 rotating disk electrode at 30 ± 1 ^oC using standard three-electrode system. A saturated calomel electrode, a Pt wire, and a catalyst modified glassy carbon electrode were used as the reference, auxiliary, and working electrodes, respectively. All potentials in the present work were referred to the reversible hydrogen electrode (RHE). The electrocatalyst modified glassy carbon working electrode was prepared according to the previously reported procedure.[44] Typically, the elelctrocatalyst ink was obtained by ultrasonic mixing 10 mg of electrocatalyst and 5 mL isopropanol/Nafion® solution (20% isopropanol and 0.02% Nafion®) for 60 min. Then, 10 μL of elelctrocatalyst ink was drop-coated on a polished glassy carbon electrode and dried at room temperature. The specific loading of electrocatalysts on the working electrode surface was about 101.9 μg cm^{-2}.

Instruments

Ultraviolet and visible spectroscopy (UV−vis) measurements were performed on Shimadzu UV2600U spectrometer. The surface charge of electrocatalyst was measured using Malvern Zetasizer Nano ZS90 zeta potential analyzer. D/max-rC X-ray diffraction (XRD), X-ray photoelectron spectroscopy (XPS, AXIS ULTRA), JSM-2010 scanning electron microscopy (SEM), JEM-2100F transmission electron microscopy (TEM), and energy dispersive X-ray (EDX) were used to characterize the chemical composition, morphology and crystal structure of samples.

Results and discussion

Characterization of Pd-NWs@PEI

Pd-NWs@PEI were achieved by reducing K_2PdCl_4 with $N_2H_4{\cdot}H_2O$ in the presence of PEI with branched structure at 80 ^oC for 2 h (see Experimental for details). The morphology of Pd-NWs@PEI was investigated by TEM. TEM images reveal the presence of abundant nanowires with the length of a few tens of nanometers and the average diameter of ca. 5 nm (Fig. 1A-B). EDX spectrum demonstrates that products mainly consist of Pd element (Fig. S1 in ESI†). The chemical state of Pd element was investigated by XPS. The mainly binding energies of Pd 3d3/2 and Pd 3d5/2 locate at 339.6 and 334.3 eV, which is indicative of metallic Pd (Fig. S2 in ESI†). Specifically, the atom percentage of metallic Pd is calculated to be ca. 86.7 % by deconvolution of the Pd 3d spectrum (Fig. S2).

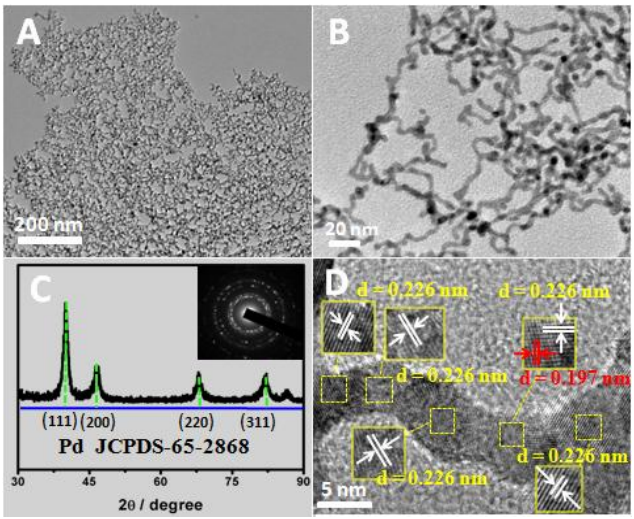

Fig. 1. (A-B) TEM images, (C) XRD pattern, and (D) HRTEM image of Pd-NWs@PEI. Insert in Fig. 1C: SAED pattern of Pd-NWs@PEI.

The crystal structure of Pd-NWs@PEI was investigated by XRD. The XRD pattern of Pd-NWs@PEI agrees well with the standard diffraction of face-centered cubic (*fcc*) Pd crystal (JCPDS-05-0681),

indicating their *fcc* structure (Fig. 1C). The selective area electron diffraction (SAED) pattern of Pd-NWs@PEI reveals the continuous diffraction rings with discrete diffraction spots, indicating their polycrystalline structure (insert in Fig. 1C). The crystal structure of Pd-NWs@PEI was further investigated by high resolution TEM (HRTEM). The interplanar distances are mainly 0.226 and 0.197 nm, corresponding to the (111) and (100) d-spacing of *fcc* Pd, confirming their polycrystalline nature. Meanwhile, the HRTEM image clearly shows the fringes are discontinuous, implying the oriented attachment grown process.[45]

The surface composition of Pd-NWs@PEI was first characterized by zeta potential, XPS, and elemental analysis. The zeta potential of Pd-NWs@PEI is ca. +40 mV at pH 5, indicating the surface of Pd-NWs@PEI contains abundant positively charged groups. XPS measurement clearly show N1s signal at 398.9 eV (Fig. S3 in ESI†), indicating the adsorption of PEI on Pd-NWs surface. At pH 5, the protonation of $-NH_2$ groups on PEI results in the high zeta potential of Pd-NWs@PEI. Our previous works demonstrate that polymeric amine can strongly bind on the Pd surface due to strong N−Pd bond.[35, 46] In order to better understand the adsorption of PEI on Pd surface, molecular dynamics (MD) simulations were carried out (see MD simulations in Supporting Information for details). MD simulations show the electron-negative N sites of PEI are attracted by Pd atoms to form an organic layer in ps time scale (Fig. 2A). Due to its branched structure, PEI only partly covers the Pd surface and form loose-packed PEI layers. Top view and side view patterns clearly show abundant holes exist in the PEI layers (Fig. 2A), through which small molecules may access the uncovered Pd atoms. To experimentally get insight into the distribution of PEI on Pd-NWs surface, elemental mapping analysis were performed on high-angle annular dark-field scanning TEM (HAADF-STEM). The Pd element pattern is very similar to the N element pattern (Fig. 2B), confirming the uniform adsorption of PEI on Pd-NWs surface through Pd-N bond. As a result, the binding energies of Pd 3d in Pd-NWs@PEI exhibit a negative shift compared to the standard value of bulk Pd (Pd $3d_{3/2}$: 340.4 eV; Pd $3d_{5/2}$: 335.1 eV[47]), originating from the strong interaction between PEI and Pd atoms (Fig. S2 in ESI†). The lone pair electrons of $-NH_2$ groups at PEI effectively donate electrons to Pd, leading to the change in the electronic property of Pd atoms.[35, 46]

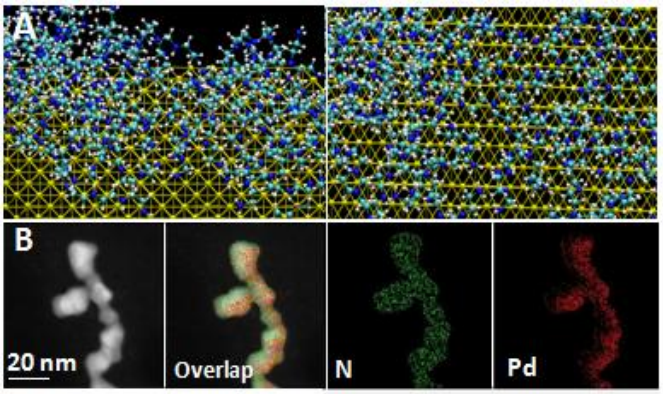

Fig. 2. (A) Side view (left) and top view (left) of configurations of adsorbed PEI on the Pd (111) surface. Pd (111) surface and PEI molecules are displayed in ball and stick style. Pd, N, C, H atoms are denoted by yellow, blue, green and white, respectively. (B) HAADF-STEM image and EDX mapping of Pd-NWs@PEI.

The formation mechanism of Pd-NWs@PEI

It is well known that the morphology of Pd nanostructures highly relates to their nucleation and crystal growth rates. Similar to the interaction between polyallylamine and K_2PdCl_4.[46] PEI with abundant $-NH_2$ groups can interact with K_2PdCl_4 to generate the light yellow PEI-Pd^{II} complex due to strong coordination ability of $-NH_2$ group (Fig. S4 and S5 in ESI†), which effectively decreases the reduction potential of Pd^{II} species (Fig. S6 in ESI†). After addition of $N_2H_4 \cdot H_2O$, UV−vis measurements show the reduction of PEI-Pd^{II} complex is completed within 2 h (Fig. 3), much lower than that (2 min) of single-component K_2PdCl_4 (Fig. S7 in ESI†). The corresponding TEM images of reaction intermediates show the morphological change from nanospheres to nanowires within the reaction time (Fig. 3B), confirming that the formation of Pd-NWs@PEI originates from the oriented attachment.[45, 48]

Since the oriented attachment involves to the aggregation of two spherical nanoparticles, the surface charge of nanoparticles will play an important role for the formation of nanowires. Thus, the solution pH of reaction system is a crucial parameter for the formation of Pd-NWs@PEI because the protonation degree of $-NH_2$ groups on Pd crystal nucleus increases with decreasing solution pH. As a result, the length of Pd-NWs@PEI decreases with the solution pH of reaction system (Fig. S8 in ESI†), which can be ascribed to the stronger electrostatic repulsion between the two PEI functionalized Pd crystal nucleus at the lower solution pH due to protonation of $-NH_2$ groups. The solution pH dependent wire's length in turn confirms the oriented attachment mechanism. Meanwhile, it is observed that the concentration of $N_2H_4 \cdot H_2O$ is also important for the synthesis of Pd-NWs. After increasing the amount of $N_2H_4 \cdot H_2O$, Pd nanonecklaces are obtained (Fig. S9 in ESI†). All Pd^{II} precursors are consumed essentially in short time due to high concentration of $N_2H_4 \cdot H_2O$ in reaction system. Thus, during oriented attachment, the further coalescence events between Pd nanoparticles on Pd nanonecklaces can't occur due to the absence of Pd^{II} precursors.

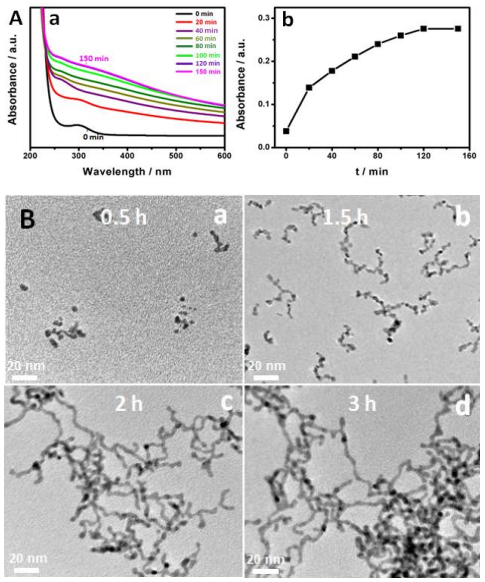

Fig. 3. (A) (a) Time-dependent UV−vis absorption spectra of the mixture solution of K_2PdCl_4 + PEI after addition of $N_2H_4 \cdot H_2O$ and (b) the corresponding plot of the absorbance intensity at 300 nm as a function of time. (B)TEM images of Pd-NWs@PEI synthesized at different reaction time: (a) 0.5, (b) 1, (c) 2, and (d) 3 h.

Electrocatalytic activity and stability of Pd-NWs@PEI for the ORR

The electrocatalytic performance of Pd-NWs@PEI was evaluated by cyclic voltammetry (CV) in a N_2-purged 0.1 M NaOH solution. For comparison, a commercial Pd black (Johnson Matthey Corporation) was also investigated under identical conditions (Fig. 4A). The ECSA of Pd electrocatalysts was measured by integrating a reduction charge of surface palladium oxide.[10, 11] The ECSA (18.8 m^2g^{-1}) of Pd-NWs@PEI is larger than that (9.6 m^2g^{-1}) of commercial Pd black, which is ascribed to the smaller particle size of Pd-NWs@PEI than Pd black (Pd-NWs@PEI: 4.7 nm vs. Pd black: 19.1 nm, Fig. S10 in ESI†). Importantly, the obvious electrochemical response confirms the PEI layers on Pd-NWs don't cover completely all Pd active sites. It is well known that thiol molecule can form self-assembled monolayers (SAMs) of alkanethiolates on Au surface. The previous works have demonstrated the straight-chain alkanethiol molecules from close-packed SAMs with$\sqrt{3}$ x$\sqrt{3}$ R 30^o unit cell whereas branched thiol molecules generally from the loose-packed SAMs (*i.e.*, the low surface coverage).[49-51] As shown in Scheme S1 in ESI†, PEI is a polymer with highly branched structure. Thus, PEI layers on Pd-NW surface should be very loose due to the steric effect, which holds most of Pd active sites of Pd-NWs due to the low surface coverage of PEI layers on Pd surface, similar to the case of branched thiolates SAMs on the Au surface.[49-51]

The ORR activities of Pd-NWs@PEI and Pd black were investigated in O_2-saturated 0.1 M NaOH solution by using rotating disk electrode (RDE) at a rotation rate of 1600 rpm (Fig. 4B). The current densities were normalized to the geometrical area of the glassy carbon working electrode. The ORR half-wave potential ($E_{1/2}$=0.865 V vs. RHE, a potential at which the current reaches half its diffusion limited value[12]) of Pd-NWs@PEI shows a positive 40 mV shift compared to that (0.825 V vs. RHE) of commercial Pd black, signifying dramatically improved ORR activity. Moreover, the $E_{1/2}$ (0.865 V vs. RHE) of Pd-NWs@PEI is higher than those of reported Pd-based nanomaterials previously, such as Pd-P nanoparticles (0.85 vs. RHE),[52] PdNi hollow nanoparticles (0.851V vs. RHE),[10] PdCu nanocubes (0.842 V vs. RHE),[14] Pd nanofowers (0.855 V vs. RHE),[26] nanoporous Pd (0.843 V vs. RHE),[53] PdRh alloy nanodendrites (0.80 V vs. RHE),[54] Au@Pd core–shell nanothorns (0.85 V vs. RHE),[55] and Pd@Ag/C composites (0.845 V vs. RHE),[56] confirming the high ORR activity of Pd-NWs@PEI. After accelerated durability test [57] (ADT, *i.e.*, potential was cycled 1000 times between 0.3 and 1.1 V vs. RHE in O_2-saturated 0.1 M NaOH solution at a scan rate of 50 mV s^{-1}), commercial Pd black shows a 21 mV degradation in $E_{1/2}$ for the ORR (Fig. S11A in ESI†) and a 48.6% loss of initial ESCA (Fig. S11B in ESI†). In contrast, the smaller degradation in $E_{1/2}$ (6 mV, Fig. S12A in ESI†) and less loss in ECSA (8.5%, Fig. S12B in ESI†) are observed at Pd-NWs@PEI, indicating the improved stability. The particular structure of nanowires effectively restrains the Ostwald ripening, which avoids the activity loss originating from the undesirable the loss of ECSA.[39, 40]

The intrinsic ORR kinetic activities (*i.e.,* the current densities were normalized to the geometrical area of the glassy carbon working electrode) of Pd-NWs@PEI and Pd black were further calculated from the ORR curves using Levich-Koutecky equation,[35] In the potential range of 0.725 to 0.975 V, the specific kinetic activity of Pd-NWs@PEI is higher than that of commercial Pd black (Fig. 4C). For example, at 0.90 V potential, the specific kinetic current density (1.594 A m^{-2}) of Pd-NWs@PEI is 6.12 times bigger than that (0.261 A m^{-2}) of Pd black (Fig. 4D). On the one hand, the interaction between PEI and Pd-NWs affects the binding energies of Pd atoms, and consequently weaken the adsorption energy of reactive intermediates (such as HO_2• and HO_2^-), which improves the ORR activity of Pd nanoparticles in alkaline media,[35, 58] On the other hand, the unique 1D wire structure of Pd-NWs@PEI acceleratess the electron transport and O_2 diffusion,[59-61] which also contributes to the improved ORR kinetics.

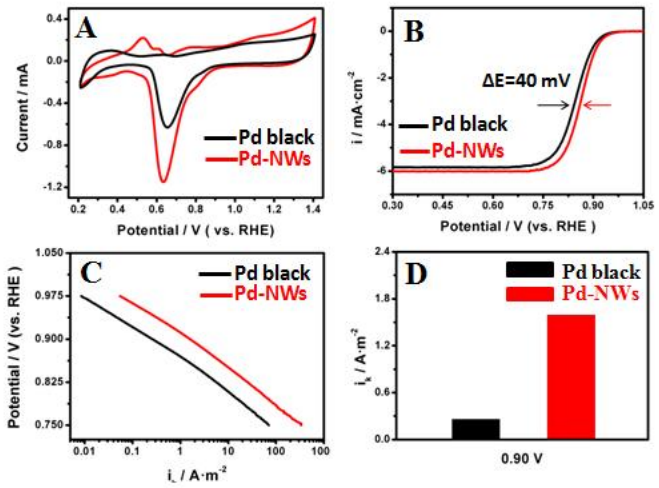

Fig. 4. (A) CV curves of Pd-NWs@PEI and commercial Pd black in N_2-saturated 0.1 M NaOH solution at a scan rate of 50 mV s^{-1}. (B) ORR polarization curves of Pd-NWs@PEI and Pd black in O_2-saturated 0.1 M NaOH solution at a scan rate of 5 mV s^{-1} and rotation rate of 1600 rpm. (C) Specific kinetic current densities (ik) for Pd-NWs@PEI and Pd black in the potential range of 0.750 to 0.975 V. (D) Specific kinetic current densities for Pd-NWs@PEI and Pd black at 0.90 V.

Electrocatalytic selectivity of Pd-NWs@PEI for the ORR

As mentioned, the development of cathodic electrocatalysts with the ORR selectivity is a critical challenge for the commercialization of DAFCs. It is clear that the size of alcohol molecule is bigger than that of oxygen molecule. As a common sense of life, we know that the window can effectively prevent large flies into the room but can't prevent the midges due to the volume difference (Scheme 1A). Since MD simulations and various characterization demonstrate that PEI layers on Pd-NWs surface has porous architecture (*i.e.*, noncompact), we infer the PEI layers on Pd-NWs surface may act as "molecular window gauze" to physically block access of alcohol molecules on Pd sites due to the larger size of alcohol molecule than oxygen molecule (ethanol: 5.1 Å vs. O_2: 3.4 Å). The alcohol resistance function of PEI layers on Pd-NWs surface first confirmed by CV in N_2-saturated 0.1 M NaOH solution with 1 M CH_3CH_2OH. The specific peak current density of Pd-NWs@PEI for the ethanol oxidation reaction is 10.8 times smaller than that of commercial Pd black (Fig. 5A), confirming the PEI layers on Pd-NWs surface can physically block access of alcohol molecules on Pd sites. Meanwhile, further CV measurements show specific activities of Pd-NWs@PEI for methanol, ethanol, and 1-propanol oxidation reactions decrease in order, relative to Pd black (Fig. S13 in ESI†), indicating specific activity of Pd-NWs@PEI decreases with increasing molecule size of

alcohol. The ORR activities of Pd-NWs@PEI and Pd black in the presence of ethanol were examined by using RDE. The obvious anodic current of ethanol oxidation is observed at the ORR polarization curve of commercial Pd black but no corresponding anodic current is observed for Pd-NWs@PEI (Fig. 5B). Meanwhile, ORR polarization measurements show the ethanol only slightly affects the ORR activity of Pd-NWs@PEI (Insert in Fig. 5B). These electrochemical results confirm PEI layers on Pd-NWs surface can effectively act as "molecular window gauze" to block the access of alcohol molecules but allow the permeation of oxygen molecules due to size difference, as shown in Scheme 1B. As a result, Pd-NWs@PEI can selectively perform the ORR in alkaline media, which makes it a promising cathodic electrocatalyst in alkaline DAFCs.

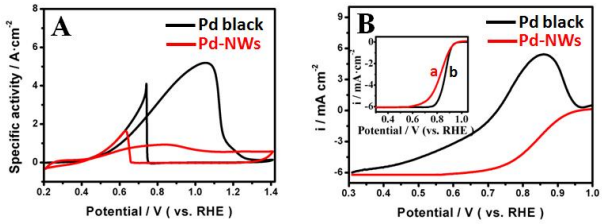

Fig. 5. (A) CV curves for Pd-NWs@PEI and Pd black in N_2-saturated 0.1 M NaOH solution with 1 M CH_3CH_2OH at a scan rate of 50 mV s^{-1}. (B) ORR polarization curves of Pd-NWs@PEI and commercial Pd black in O_2-saturated 0.1 M NaOH solution with 1 M CH_3CH_2OH at a scan rate of 5 mV s^{-1} and rotation rate of 1600 rpm. Insert: the comparison of ORR polarization curves of Pd-NWs@PEI in O_2-saturated 0.1 M NaOH solution (a) with and (b) without the presence of 1 M CH_3CH_2OH at a scan rate of 5 mV s^{-1} and rotation rate of 1600 rpm.

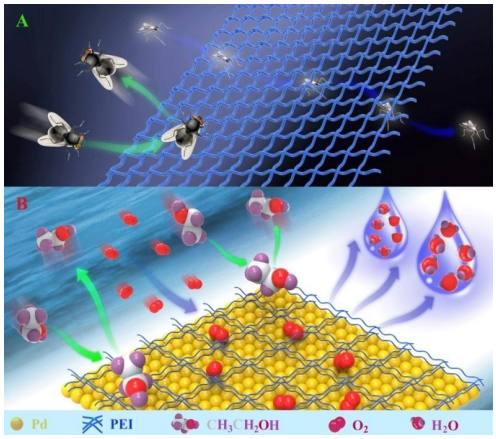

Scheme 1 (A) Schematic illustration on the selectivity of window gauze for the fly and midge. (B) Schematic mechanism for the ORR selectivity of Pd-NWs@PEI in the presence of ethanol.

Conclusions

In summary, a facile and wet-chemical synthetic procedure of chemical functionalized Pd-NWs was developed by using PEI as the complexant and functional molecules. Owing to its branched structure, PEI couldn't form the compact layers on Pd-NWs surface, resulting in the formation of "molecular window gauze" on Pd-NWs surface. Thus, Pd-NWs@PEI achieved the high ORR selectivity in alkaline media by physically blocking the accessibility of ethanol with large molecular size on Pd sites. Meanwhile, PEI functionaliztion modified the surface electronic structure of Pd-NWs, resulting in the enhanced ORR activity. Additionally, the particular one-dimensional structure of Pd-NWs effectively restrained the Ostwald ripening, endowing Pd-NWs@PEI with the improved ORR stability. We anticipated that this chemical functionalization strategy could be applied generally to other noble metal electrocatalysts with improved electrocatalytic selectivity and activity.

Acknowledgements

This research was sponsored by National Natural Science Foundation of China (21473111 and 21473107), Natural Science Foundation of Shaanxi Province (2015JM2043), and Fundamental Research Funds for the Central Universities (GK201402016).

Notes and references

1. N. Kakati, J. Maiti, S. H. Lee, S. H. Jee, B. Viswanathan and Y. S. Yoon, *Chem. rev.*, 2014, **114**, 12397.
2. X. Zhao, M. Yin, L. Ma, L. Liang, C. P. Liu, J. H. Liao, T. H. Lu and W. Xing, *Energy Environ. Sci.*, 2011, **4**, 2736.
3. L. Nguyen Viet, Y. Yang, T. Cao Minh, M. Nguyen Van, Y. Cao and M. Nogami, *Nano Energy*, 2013, **2**, 636.
4. R. Wang, J. Liu, P. Liu, X. Bi, X. Yan, W. Wang, X. Ge, M. Chen and Y. Ding, *Chem. Sci.*, 2014, **5**, 403.
5. A. Oh, H. Baik, D. S. Choi, J. Y. Cheon, B. Kim, H. Kim, S. J. Kwon, S. H. Joo, Y. Jung and K. Lee, *ACS Nano*, 2015, **9**, 2856.
6. Q. Jia, W. Liang, M. K. Bates, P. Mani, W. Lee and S. Mukerjee, *ACS Nano*, 2015, **9**, 387.
7. L. Zhang, M. Wei, S. Wang, Z. Li, L.-X. Ding and H. Wang, *Chem. Sci.*, 2015, **6**, 3211.
8. Y. M. Tan, C. F. Xu, G. X. Chen, N. F. Zheng and Q. J. Xie, *Energy Environ. Sci.*, 2012, **5**, 6923.
9. S. B. Yin, M. Cai, C. X. Wang and P. K. Shen, *Energy Environ. Sci.*, 2011, **4**, 558.
10. M. Wang, W. Zhang, J. Wang, D. Wexler, S. D. Poynton, R. C. Slade, H. Liu, B. Winther-Jensen, R. Kerr and D. Shi, *ACS appl. mater. inter.*, 2013, **5**, 12708.
11. Z. Y. Zhang, K. L. More, K. Sun, Z. L. Wu and W. Z. Li, *Chem. Mater.*, 2011, **23**, 1570.
12. Y. Lu, Y. Jiang, X. Gao, X. Wang and W. Chen, *J. Am. Chem. Soc.*, 2014, **136**, 11687.
13. L. Xu, Z. Luo, Z. Fan, X. Zhang, C. Tan, H. Li, H. Zhang and C. Xue, *Nanoscale*, 2014, **6**, 11738.
14. Q. Gao, Y. M. Ju, D. An, M. R. Gao, C. H. Cui, J. W. Liu, H. P. Cong and S. H. Yu, *ChemSusChem*, 2013, **6**, 1878.
15. M. Liu, Y. Lu and W. Chen, *Adv. Funct. Mater.*, 2013, **23**, 1289.
16. S. M. Alia, K. Duong, T. Liu, K. Jensen and Y. Yan, *ChemSusChem*, 2014, **7**, 1739.
17. G. Hu, F. Nitze, E. Gracia-Espino, J. Ma, H. R. Barzegar, T. Sharifi, X. Jia, A. Shchukarev, L. Lu, C. Ma, G. Yang and T. Wågberg, *Nat. Commun.*, 2014, **5**, 5253.
18. W.-P. Wu, A. P. Periasamy, G.-L. Lin, Z.-Y. Shih and H.-T. Chang, *J. Mater. Chem. A*, 2015, **3**, 9675.
19. S.-S. Li, A.-J. Wang, Y.-Y. Hu, K.-M. Fang, J.-R. Chen and J.-J. Feng, *J. Mater. Chem. A*, 2014, **2**, 18177.
20. L.-L. He, P. Song, A.-J. Wang, J.-N. Zheng, L.-P. Mei and J.-J. Feng, *J. Mater. Chem. A*, 2015, **3**, 5352.
21. Y. Zheng, S. Zhao, S. Liu, H. Yin, Y.-Y. Chen, J. Bao, M. Han and Z. Dai, *ACS appl. mater. inter.*, 2015, **7**, 5347.
22. D. D. Vaughn II, J. Araujo, P. Meduri, J. F. Callejas, M. A. Hickner and R. E. Schaak, *Chem. Mater.*, 2014, **26**, 6226.

23. L. Arroyo-Ramírez, R. Montano-Serrano, T. Luna-Pineda, F. l. R. Román, R. G. Raptis and C. R. Cabrera, *ACS appl. mater. inter.*, 2013, **5**, 11603.
24. J. H. Shim, J. Kim, C. Lee and Y. Lee, *Chem. Mater.*, 2011, **23**, 4694.
25. P. Kannan, T. Maiyalagan and M. Opallo, *Nano Energy*, 2013, **2**, 677.
26. Q. Gao, M.-R. Gao, J.-W. Liu, M.-Y. Chen, C.-H. Cui, H.-H. Li and S.-H. Yu, *Nanoscale*, 2013, **5**, 3202.
27. Q. Shi, P. Zhang, Y. Li, H. Xia, D. Wang and X. Tao, *Chem. Sci.*, 2015, **6**, 4350.
28. J. R. C. Salgado, E. Antolini and E. R. Gonzalez, *Appl. Catal. B-Environ.*, 2005, **57**, 283.
29. J. H. Yang, W. J. Zhou, C. H. Cheng, J. Y. Lee and Z. L. Liu, *Acs Appl. Mater. Inter.*, 2010, **2**, 119.
30. K. Kamiya, R. Kamai, K. Hashimoto and S. Nakanishi, *Nat. commun.*, 2014, **5**, 5040.
31. H. Liu, J. Qu, Y. Chen, J. Li, F. Ye, J. Y. Lee and J. Yang, *J. Am. Chem. Soc.*, 2012, **134**, 11602.
32. Z. Wu, Y. Lv, Y. Xia, P. A. Webley and D. Zhao, *J. Am. Chem. Soc.*, 2012, **134**, 2236.
33. B. Genorio, R. Subbaraman, D. Strmcnik, D. Tripkovic, V. R. Stamenkovic and N. M. Markovic, *Angew. Chem. Int. Edit.*, 2011, **50**, 5468.
34. B. Genorio, D. Strmcnik, R. Subbaraman, D. Tripkovic, G. Karapetrov, V. R. Stamenkovic, S. Pejovnik and N. M. Markovic, *Nat. Mater.*, 2010, **9**, 998.
35. G. Fu, X. Jiang, L. Tao, Y. Chen, J. Lin, Y. Zhou, Y. Tang and T. Lu, *Langmuir*, 2013, **29**, 4413.
36. F. Ksar, G. Surendran, L. Ramos, B. Keita, L. Nadjo, E. Prouzet, P. Beaunier, A. Hagege, F. Audonnet and H. Remita, *Chem. Mater.*, 2009, **21**, 1612.
37. C. Xu, H. Wang, P. K. Shen and S. P. Jiang, *Adv. Mater.*, 2007, **19**, 4256.
38. J. Zhang, Y. Xu and B. Zhang, *Chem. Commun.*, 2014, **50**, 13451.
39. H. Liu, C. Koenigsmann, R. R. Adzic and S. S. Wong, *ACS Catal.*, 2014, **4**, 2544.
40. C. Koenigsmann and S. S. Wong, *ACS Catal.*, 2013, **3**, 2031.
41.Y. Wang, S.-I. Choi, X. Zhao, S. Xie, H.-C. Peng, M. Chi, C. Z. Huang and Y. Xia, *Adv. Funct. Mater.*, 2014, **24**, 131.
42. C. Koenigsmann, E. Sutter, T. A. Chiesa, R. R. Adzic and S. S. Wong, *Nano Lett.*, 2012, **12**, 2013.
43. C. Koenigsmann, A. C. Santulli, E. Sutter and S. S. Wong, *Acs Nano*, 2011, **5**, 7471.
44. Y. Garsany, O. A. Baturina, K. E. Swider-Lyons and S. S. Kocha, *Anal. Chem.*, 2010, **82**, 6321.
45. J. Xu, G. Fu, Y. Tang, Y. Zhou, Y. Chen and T. Lu, *J. Mater. Chem.*, 2012, **22**, 13585.
46. G. Fu, W. Han, L. Yang, J. Lin, S. Wei, Y. Chen, Y. Zhou, Y. Tang, T. Lu and X. Xia, *J. Mater. Chem.*, 2012, **22**, 17604.
47. J. Moulder, W. Stickle, P. Sobol and K. Bomben, Handbook of X-ray Photoelectron Spectroscopy, Perkin-Elmer Corporation, Physical Electronics Division: Eden Prairie, MN, 1992.
48. M. Xiao, S. Li, J. Zhu, K. Li, C. Liu and W. Xing, *ChemPlusChem*, 2014, **79**, 1123-1128.
49. V. Chechik, H. Schönherr, G. J. Vancso and C. J. M. Stirling, *Langmuir*, 1998, **14**, 3003.
50. Y.-S. Shon, R. Colorado, C. T. Williams, C. D. Bain and T. R. Lee, *Langmuir*, 2000, **16**, 541.
51. Chi, J. Zhang and J. Ulstrup, *J. Phys. Chem. B*, 2006, **110**, 1102.
52. K. C. Poon, D. C. Tan, T. D. Vo, B. Khezri, H. Su, R. D. Webster and H. Sato, *J. Am. Chem. Soc.*, 2014, **136**, 5217.
53. J. H. Shim, Y. S. Kim, M. Kang, C. Lee and Y. Lee, *Phys. Chem. Chem. Phys.*, 2012, **14**, 3974.
54. Y. Qi, J. Wu, H. Zhang, Y. Jiang, C. Jin, M. Fu, H. Yang and D. Yang, *Nanoscale*, 2014, **6**, 7012.
55. G. Fu, Z. Liu, Y. Chen, J. Lin, Y. Tang and T. Lu, *Nano Res.*, 2014, **7**, 1205-1214.
56. L. Jiang, A. Hsu, D. Chu and R. Chen, *Electrochim. Acta*, 2010, **55**, 4506.
57. B. Lim, M. J. Jiang, P. H. C. Camargo, E. C. Cho, J. Tao, X. M. Lu, Y. M. Zhu and Y. N. Xia, *Science*, 2009, **324**, 1302.
58. J. S. Spendelow and A. Wieckowski, *Phys. Chem. Chem. Phys.*, 2007, **9**, 2654.
59. S. H. Sun, G. X. Zhang, D. S. Geng, Y. G. Chen, R. Y. Li, M. Cai and X. L. Sun, *Angew. Chem. Int. Edit.*, 2011, **50**, 422.
60. B. Y. Xia, W. T. Ng, H. Bin Wu, X. Wang and X. W. Lou, *Angew. Chem. Int. Edit.*, 2012, **51**, 7213.
61. C. Koenigsmann and S. S. Wong, *Energy Environ. Sci.*, 2011, **4**, 1161.

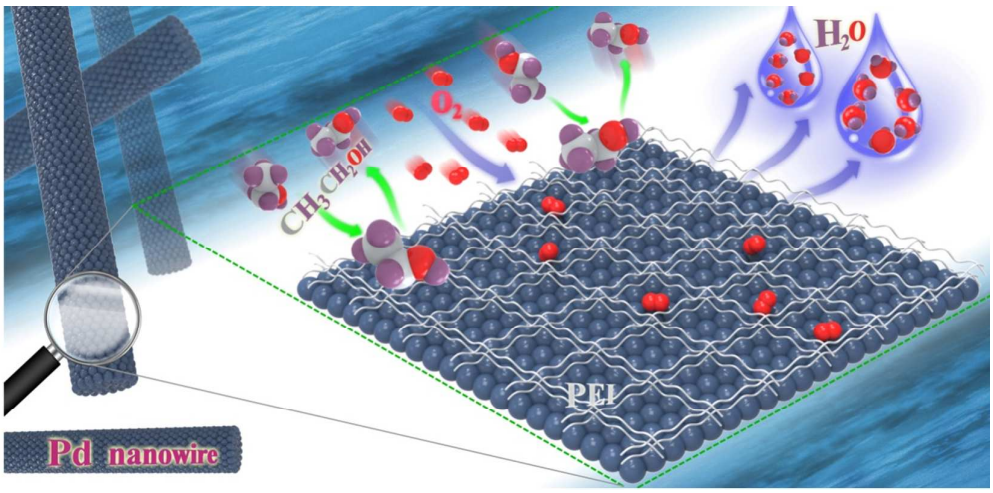

Polyethyleneimine layers on Pd nanowires act as “molecular window gauze”, resulting in good selectivity for the ORR in alkaline media.